13èmes Journées de l'Hydrodynamique
21 - 23 novembre 2012
Laboratoire d'Hydraulique Saint-Venant
Ile des Impressionnistes,
Chatou (78), France

Reconstruction et prédiction d'états de mer à l'aide d'observations spatio-temporelles de la surface par une caméra LIDAR

Reconstruction and prediction of sea surface state with spatio-temporal observations of the sea surface by a LIDAR camera

F. NOUGUIER*, S. GRILLI, C.-A. GUERIN***

* Institut Méditerranéen d'Océanologie
Université du Sud-Toulon-Var, Avenue de l'université, BP 20132 F-83957 La garde cedex
** Department of Ocean Engineering
University of Rhode Island, Narragansett, RI, USA
frederic.nouguier@univ-tln.fr

Résumé

L'étude présentée porte sur le développement d'un algorithme de reconstruction de la surface libre de la mer à partir d'observations spatio-temporelle discrètes de celle-ci au moyen d'une caméra Flash LIDAR. Nous supposons pour l'étude que la caméra est montée sur un navire et observe à une centaine de mètres à l'avant de celui-ci. Les positions de la surface libre sont recueillies sur l'avant de la trajectoire du navire. La géométrie est telle que la densité des observations décroit rapidement avec la distance d'observation. L'algorithme de reconstruction a premièrement été développé dans le cas de surfaces aléatoires linéaires uni- et bi-dimensionelles dont les amplitude des coefficients la décrivant ont été obtenues à l'aide d'une minimisation par moindre carrés de l'erreur entre les observations et la surface reconstruite. Dans les cas tests présentés, les surfaces aléatoires ont été générées à l'aide du spectre de Pierson-Moskowitz ou d'Elfouhaily et les jeux de données d'observations ont été obtenus par le calcul des intersections géométriques des rayons laser avec les surfaces simulées. Une fois la reconstruction de la surface opérée, une prévision du profil des vagues à l'avant du navire est possible. Celle-ci est calculée sur une fenêtre temporelle dépendant non seulement de la durée d'initialisation/d'observation mais également des longueurs d'onde de vagues qui auront été correctement reconstruites par l'algorithme. Cependant, pour des états de mer avancés, les effets nonlinéaires se doivent d'être également pris en compte pour une meilleure reconstruction. Le modèle Lagrangien "Choppy wave model" ([6]) est utilisé à cet effet et permet une amélioration nécessaire de l'algorithme d'inversion.

Summary

We report on the development of free surface reconstruction algorithms to predict ocean waves, based on spatial observations made with a high frequency Flash LIDAR camera. We assume that the camera is mounted on a vessel, in a forward looking position, and is pointing at some distance ahead of its path yielding a sample of spatio-temporal wave elevation data. Due to the geometry, the density of measurement points gradually decreases (i.e., becomes sparse) with the distance to the camera. Free surface reconstruction algorithms were first developed and validated for linear 1D and 2D irregular surface models, whose amplitude coefficients are estimated based on minimizing the mean square error of simulated surface elevations to measurements, over space and time (for a specified time initialization period). In the validation tests reported here, irregular ocean surfaces are generated based on a directional Pierson-Moskowitz or Elfouhaily spectrum, and simulated LIDAR data sets are constructed by performing geometric intersections of laser rays with each generated surface. Once a nowcast of the ocean surface is estimated from the (simulated) LIDAR data, a forecast can be made of expected waves ahead of the vessel, for a time window that depends both on the initialization period and the resolved wavenumbers in the reconstruction. The process can then be repeated for another prediction window, and so forth. To reconstruct severe sea states, however, nonlinear effects must be included in the sea surface representation. This is done, here, by representing the ocean surface using the efficient Lagrangian "Choppy wave model"([6]).

I – Introduction

In many ocean engineering applications where ocean wave information is needed, it is often sufficient to use phase-averaged wave data, usually in the form of a directional wave energy spectrum. For some applications, however, both more accurate and detailed phase resolved, real time, wave data is required. This is for instance the case when predicting seakeeping and anticipating the motions of a surface vessel, based on measurements of the ocean surface made ahead of its trajectory. In such a case, the free surface must be reconstructed in real time from a limited number of measurements, which requires applying so-called free surface reconstruction algorithms.

In the last decade new techniques have been proposed in the microwave domain for the reconstruction of surface elevation maps ([4], [2], [5], [1]), using radar systems at grazing incidence angles. Here, we report on the development and application of reconstruction and prediction algorithms for the ocean surface, based on spatio-temporal data acquired at high frequency by a Flash LIDAR camera. A FLC generates a $n \times n$ matrix of laser rays, providing n^2 simultaneous measurements of the distance from the FLC to the ocean surface. The camera can be mounted on a vessel (on top of a mast), in a forward looking position, pointing at some distance ahead of its path. From the measured data and the camera's location and orientation, as well as known vessel's motions, the elevation and horizontal position of the measured surface points can be generated in an absolute coordinate system.

Since laser rays are first reflecting off of the nearest ocean wave crests, the density of measurement points inevitably gradually decreases with the distance to the camera even if the horizontal sampling is regular. Hence, this results in a highly spatially non-uniform distribution of ocean surface elevation values/data (as, e.g., sketched in Fig. 1), as a function of time (i.e., a spatio-temporal data set), based on which the ocean surface must be reconstructed.

While a linear reconstruction should be sufficient for the short term forecast of moderate sea states, to better estimate more severe sea states and predict them later in time, nonlinear effects must be included in the sea surface representation. The existing nonlinear models, however, were all quite computationally demanding, particularly in a reconstruction mode. Here, we represent nonlinear sea surfaces using the efficient Lagrangian model Choppy Wave (CW), which was demonstrated to correctly approximate second-order properties of waves with narrow-banded spectra ([6]) and to be accurate enough for most sea states, as long as there are limited to decimeter gravity waves. The CW model is used in the proposed reconstruction algorithms.

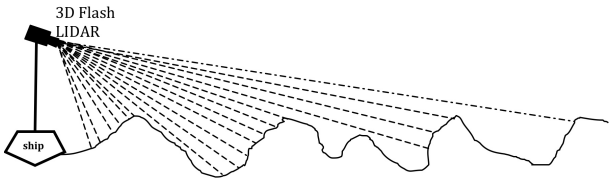

Figure 1 – Sketch of flash-LIDAR angle of view of the ocean surface and visualization of a few rays (1D situation). Measurement points are sparse far from the ship.

II – Ocean Free Surface Representation

In this work, we consider ocean surface representations based either on linear superposition of independant waves ([3]) or on the nonlinear CW model, which is an extension of Gertsner's wave theory ([6]). k_n is defined as a wavenumber (wavelength λ_n) and ω_n the circular frequency. In deep water, the dispersion relationship writes : $\omega_n^2 = gk_n$.

Hence, the linear superposition of $n = 1, \ldots, N$ individual wave harmonics of elevation A_n and direction Θ_n yields the linear ocean surface representation, in the horizontal plane of coordinates $\boldsymbol{x} = (x, y)$,

$$\eta(\boldsymbol{x}, t) = \sum_{n=1}^{N} A_n \cos\left(\Psi_n - \varphi_n\right) \;\; ; \;\; \Psi_n = k_{nx}x + k_{ny}y - \omega_n t \tag{1}$$

where Ψ_n are spatio-temporal phase functions, $\varphi_n = 2\pi\mathcal{R}_n$ are mutually independent (i.e., random) phases, with $\mathcal{R}_n \in [0, 1]$ a set of uniformly distributed random numbers, and $(k_{xn}, k_{yn}) = k_n\{x\,\cos\Theta_n + y\,\sin\Theta_n\} = \boldsymbol{k}_n \cdot \boldsymbol{x}$, with $\boldsymbol{k}_n = k_n(\cos\Theta_n, \sin\Theta_n) = k_n\hat{\boldsymbol{k}}_n$, with $\hat{\boldsymbol{k}}_n = (\cos\Theta_n, \sin\Theta_n)$, the unit wavenumber vectors (where $\Theta_n \in [0, 2\pi]$ denotes a direction of propagation).

To simplify the following mathematical and algorithm developments, related to free surface reconstruction, it is more convenient (and numerically accurate) to use the equivalent linear representation,

$$\eta(\boldsymbol{x}, t) = \sum_{n=1}^{N} |k_n|^{-3/2} \left\{a_n \cos\Psi_n + b_n \sin\Psi_n\right\} \tag{2}$$

where $\{a_n, b_n; n = 1, \ldots, N\}$ are $2N$ wave harmonic parameters describing the ocean surface, with,

$$a_n = |k_n|^{3/2} A_n \cos\varphi_n \;\; ; \;\; b_n = |k_n|^{3/2} A_n \sin\varphi_n \tag{3}$$

The factors $|k_n|^{-3/2}$ constitute a preconditioning, which anticipates the fact that the harmonic amplitude coefficients are related to the square root of the energy density spectrum (see below). This preconditioning will make for better conditioned matrices in the reconstruction algorithms discussed later.

The CW ocean surfaces are obtained from linear surfaces, such as Eq. (2), based on the transformation,

$$(\boldsymbol{x}, \eta(\boldsymbol{x}, t)) \rightarrow (\boldsymbol{x} + \boldsymbol{D}(\boldsymbol{x}, t), \eta(\boldsymbol{x}, t)) \tag{4}$$

where $\boldsymbol{D}(\boldsymbol{x}, t)$ is the spatial Riez Transform (Hilbert Transform in 1D) of η. It can be shown ([6]) that this transformation introduces a phase quadrature with respect to the original signal ; hence, it writes,

$$\boldsymbol{D}(\boldsymbol{x}, t) = \sum_{n=1}^{N} |k_n|^{-3/2} \left\{-a_n \sin\Psi_n + b_n \cos\Psi_n\right\} \hat{\boldsymbol{k}}_n \tag{5}$$

The nonlinear surface, $\tilde{\eta}$ is thus implicitly defined as

$$\tilde{\eta}(\boldsymbol{x} + \boldsymbol{D}(\boldsymbol{x}, t), t) = \eta(\boldsymbol{x}, t) \tag{6}$$

In the ocean, we assume that the wave amplitude of each component can be found from a (discretized) directional energy density spectrum $S(\mathbf{k}_n) = S(k_n, \Theta_n)$ such as,

$$A_n = \sqrt{2S(k_n, \Theta_n)\, k_n \Delta k\, \Delta\Theta} \tag{7}$$

In the following applications, when generating ocean surfaces (whether linear or nonlinear), we will either assume an omnidirectional discrete Pierson-Moskowitz spectrum (PM) for fully developed open seas, or a directional discrete Elfouhaily spectrum (EY).

III – Free Surface Reconstruction Algorithms

Assuming a set of observations of the free surface elevation made at M times, using a LIDAR camera with J active rays (i.e., actually intersecting the free surface), i.e., $\eta_{j,m} = \eta(\boldsymbol{x}_j, t_m); l = j, \ldots, J; m = 1, \ldots, M$, one wishes to reconstruct the ocean surface geometry over some specified range of wavelengths : $(\lambda^r_{min}, \lambda^r_{max})$. In the following, we present reconstruction algorithms based on a linear or 2nd-order (Choppy) representation of the free surface. These consist in optimizing the values of $2N$ unknown parameters (a_n, b_n) by minimizing a cost function expressing the Root Mean Square (RMS) difference between the reconstructed surface values and the observations.

We validate the proposed algorithms using numerically simulated LIDAR data, extracted from randomly generated ocean surfaces (i.e., linear or Choppy), having a specified wave energy spectrum as detailed in the above section. In the validation applications, both 1D and 2D (linear or Choppy) cases will be presented and discussed.

III – 1 Linear Ocean Free Surface Reconstruction

Here, we assume that the ocean surface is represented by Eq. (2). The simplest minimization of differences between model and observations can be achieved through applying a straightforward Least Square Method (LSM). To do so, we define a cost function for the measured spatio-temporal data points η_l $(l = 1, \ldots, L = J \cdot M)$ as,

$$C = \frac{1}{L} \sum_{l=1}^{L} \left(\eta(\boldsymbol{x}_l, t_l) - \eta_l\right)^2 \tag{8}$$

where $\eta(\boldsymbol{x}_l, t_l)$ are the unknown reconstructed surface elevations and η_l are the observations. An extremum of this function is reached for,

$$\frac{\partial C}{\partial a_m} = 0, \ \frac{\partial C}{\partial b_m} = 0 \ ; \ m = 1, .., N \tag{9}$$

Developing these equations yields a linear system of $2N$ equations for $2N$ unknown parameters $(m = 1, \ldots, N)$,

$$\begin{aligned}
\sum_{l=1}^{L} \sum_{n=1}^{N} |k_n|^{-3/2} \{ a_n \cos\Psi_{ml} \cos\Psi_{nl} \ + \ b_n \cos\Psi_{ml} \sin\Psi_{nl} \} &= \sum_{l=1}^{L} \eta_l \cos\Psi_{ml} \\
\sum_{l=1}^{L} \sum_{n=1}^{N} |k_n|^{-3/2} \{ a_n \sin\Psi_{ml} \cos\Psi_{nl} \ + \ b_n \sin\Psi_{ml} \sin\Psi_{nl} \} &= \sum_{l=1}^{L} \eta_l \sin\Psi_{ml}
\end{aligned} \tag{10}$$

where wave harmonic phases are defined as, $\Psi_{nl} = \boldsymbol{k}_n \cdot \boldsymbol{x}_l - \omega_n t_l$. This linear system can be recast in matrix form as

$$A_{mn} X_n = B_n \ \ ; \ \ X_n = [a_1..a_N, b_1..b_N] \tag{11}$$

where X_n is a vector made of the $2N$ unknown parameters,

$$B_n = \left\{ \begin{array}{l} \sum_{l=1}^{L} \eta_l \cos\Psi_{nl};\ 1 \le n \le N \\ \sum_{l=1}^{L} \eta_l \sin\Psi_{nl};\ N+1 \le n \le 2N \end{array} \right\} \tag{12}$$

and, A_{mn} the $2N \times 2N$ matrix

$$\begin{aligned} A_{mn} &= \sum_{l=1}^{L} |k_n|^{-3/2} \cos\Psi_{ml} \cos\Psi_{nl} \\ A_{m,N+n} &= \sum_{l=1}^{L} |k_n|^{-3/2} \cos\Psi_{ml} \sin\Psi_{nl} \\ A_{N+m,n} &= \sum_{l=1}^{L} |k_n|^{-3/2} \sin\Psi_{ml} \cos\Psi_{nl} \\ A_{N+m,N+n} &= \sum_{l=1}^{L} |k_n|^{-3/2} \sin\Psi_{ml} \sin\Psi_{nl} \end{aligned} \tag{13}$$

The linear system (11) is solved at each step of data acquisition using either the direct Gauss elimination method or, for larger systems, the more efficient iterative method GMRES.

III – 2 Choppy Ocean Free Surface Reconstruction

Here, we assume that the ocean surface is represented by Eq. (6), using the definition of $\boldsymbol{D}$ in Eq. (5). As before, we use a quadratic cost function to optimize the reconstructed surface amplitude parameters (a_n, b_n) with respect to $L = M \cdot J$ spatio-temporal observations η_l, as,

$$\tilde{C} = \frac{1}{L} \sum_{l=1}^{L} \left(\tilde{\eta}(\boldsymbol{y}_l, t_l) - \eta_l \right)^2 \tag{14}$$

where $\boldsymbol{y}_l$, in this case, are the horizontal coordinates of the set of observations points on the surface. For each $\boldsymbol{y}_l$ we can find $\boldsymbol{x}_l$ such that,

$$\boldsymbol{y}_l = \boldsymbol{x}_l + \boldsymbol{D}(\boldsymbol{x}_l, t_l) \tag{15}$$

Using this equation in (14) and the implicit definition (6) of the nonlinear surface, we recast the cost function as,

$$\tilde{C} = \frac{1}{L} \sum_{l=1}^{L} \left(\eta(\boldsymbol{x}_l, t_l) - \eta_l \right)^2 \tag{16}$$

where η is the underlying linear surface taken at the horizontal coordinates $\boldsymbol{x}_l$.

The extremum condition is thus still defined by Eq. (9), which results in the same linear system of equations with however the important difference that now η_l and η are elevations taken at different horizontal coordinates. As $\boldsymbol{D}$ and thus $\boldsymbol{x}_l$ and all Ψ_{nl} are unknown, we need to proceed iteratively to find them jointly with η. Since in Choppy the nonlinear surface is close to the linear one, we begin the iterative process by assuming that $\boldsymbol{x}_l^{(0)} = \boldsymbol{y}_l$ (i.e., $\boldsymbol{D} = 0$). Solving the system of equations yields a first solution $(\tilde{a}_n^{(0)}, \tilde{b}_n^{(0)})$,

which allows deriving a better estimate of $\boldsymbol{x}_l$: $\boldsymbol{x}_l^{(1)} = \boldsymbol{y}_l - \boldsymbol{D}^{(0)}(\boldsymbol{x}_l^{(0)}, t_l)$. This iterative process can thus formally be defined as,

$$\boldsymbol{x}_l^{(n+1)} = \boldsymbol{y}_l - \boldsymbol{D}^{(n)}(\boldsymbol{x}_l^{(n)}, t_l) \quad \underset{(a)}{\longrightarrow} \quad (\tilde{a}_n^{(n+1)}, \tilde{b}_n^{(n+1)}) \quad \underset{(b)}{\longrightarrow} \quad (\eta^{(n+1)}, \boldsymbol{D}^{(n+1)}) \tag{17}$$

where superscripts in parentheses refer to the iteration number. Step (a) is achieved by solving the system (11) and step (b) via applying the definition in Eqs. (2) and (5). It should be noted that the first step is equivalent to a linear reconstruction. In practice, convergence is reached after only a few iterations. Hence, a nonlinear inversion usually takes 3 or 4 times longer to compute than a linear inversion.

IV – Reconstruction and prediction of 1D surfaces

IV – 1 The effect of nonlinearities on nowcast and forecast

In this first part, we assume that the data set of observations is constituted of all the points used for numerically generating the ocean surface. A nonlinear ocean surface is generated using Choppy, assuming a PM spectrum with a wind speed $U_{19.5} = 10$ m.s^{-1}, yielding a dominant wavelength $\lambda_p = 83.3$ m and wavenumber $k_p = 0.075$ m^{-1} (Eq. (**??**)). A linear surface is first generated using the random phase method, by way of a Fast Fourier Transform with 1024 points over 200 m (Eqs. (1) and (7)), and then transformed into a nonlinear surface by applying the Choppy transformation (4).

Both linear and nonlinear free surface reconstructions are performed with $N_k = 400$ wavenumbers k_n, and 10 iterations are used in the nonlinear reconstruction. The reconstructed wavenumber vector is logarithmically spaced in between $k_{min} = 2\pi/\lambda_{max}$ and $k_{max} = 2\pi/\lambda_{min}$, with $\lambda_{max} = 90$ m and $\lambda_{min} = 2$ m. The observation data set used in the reconstruction is the whole surface sampling (i.e., with 1024 points). Figure 2(a) shows a zoom on the simulated and the linear and nonlinear reconstructed surfaces.

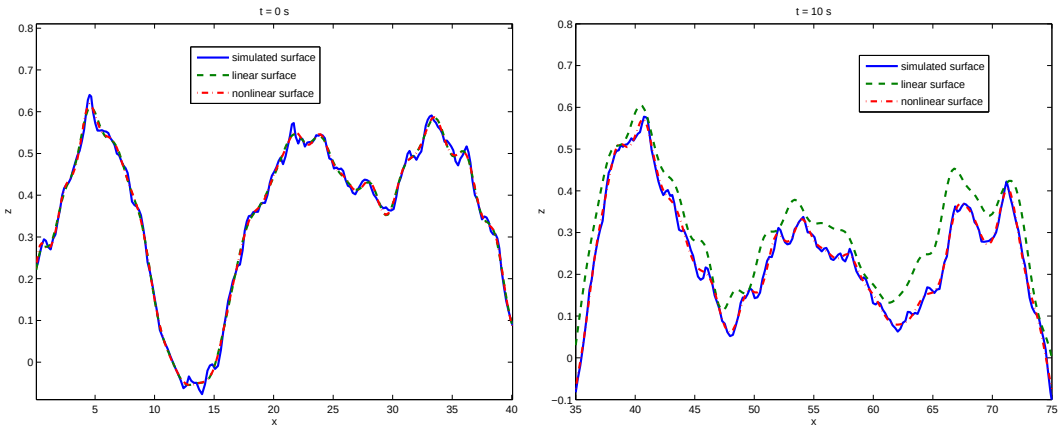

(a) (b)

Figure 2 – Linear and nonlinear reconstructions of a time evolving 1D CWM surface : a) at initial inversion time ($t = 0$ s) ; b) at the forcasted surface time ($t = 10$ s)

Because our reconstruction methodology relies on a cost function minimization, we observe a very good reconstruction at the first time step $t = 0$ s (Fig. 2(a)), in both linear and nonlinear cases. Figure 2(b) shows the time evolution (i.e., forecast) at $t = 10$ s of the reference and reconstructed linear and nonlinear surfaces, obtained by time updating

the phase functions Ψs. Figure 3 shows the relative error of the two reconstructions as a function of the forecasting time. In the figure, errors have been averaged over 10 surfaces both for statistical purpose and to provide smoother curves. As expected, the nonlinear inversion provide a more accurate estimation of the propagated surface at forecasted times. In the presented case, relative error is eight times smaller in the nonlinear inversion.

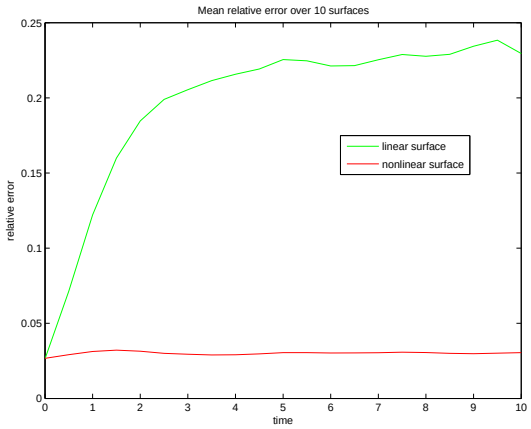

Figure 3 – Relative error of the two reconstructions as a function of the forecasting time.

IV – 2 Generation and Reconstruction using 1D LIDAR Data

Here, we consider the same sea state as used earlier, described by a PM spectrum with $U_{19.5} = 10$ m.s^{-1}, and create a simulated LIDAR data set by calculating the geometric intersections of a series of LIDAR rays with one-dimensional (1D) simulated free surfaces, as a function of space and time (e.g., Fig. 4). The spectrum has been cut-off in the lower and higher wavenumber ranges such as $k_{min} = 2\pi/w$ and $k_{max} = 2\pi/dr$, where $w = 200$ m and $dr = 0.20$ m are the surface length and the spatial sampling, respectively. The surface length was selected to be larger than the peak spectral wavelength $\lambda_p = 83.3$ m, and dr is such that $\lambda_{min} = 2 \times dr$, the minimum wavelength present on the free surface. In the following, we also assume that the LIDAR camera is located at $z_0 = 10$ m above the ocean mean water level, with its main axis of view pointing at a distance $d_0 = 100$ m ahead. The vertical aperture is $\theta_v = 13$ deg. and there are $n_{rv} = 64$ rays in the vertical plane. The LIDAR can acquire simultaneous spatial data sets, at up to a 20 Hz frequency (i.e., every 0.05 s).

Ocean surfaces are generated based on the PM spectrum, as before, using a random phase method. Here, we use $N = 1024$ individual wavenumbers distributed over the selected range, with 512 positive and negative k values.

Figure 5 shows the interface reconstruction algorithm results of simulated LIDAR data obtained from a unique snapshot of a linear ocean surface. We use $N_k = 40$ or 400 wavenumbers, logarithmically spaced between 0.07 and 3.1 rad.m^{-1} ($\lambda_{max} = 90$ m and $\lambda_{min} = 2$ m), respectively, in the linear reconstruction algorithm results shown in Figs. 5(a) and 5(b). Black dots represent the data set of simulated observations. No additional noise, representing experimental errors, is included at this stage. As expected, the reconstruction is very accurate over the LIDAR footprint area but the algorithm fails to reconstruct the surface outside this zone, where the inversion process is not constrained. The footprint area size is thus a major parameter and should be carefully defined as a function of the desired reconstructed wavelength interval.

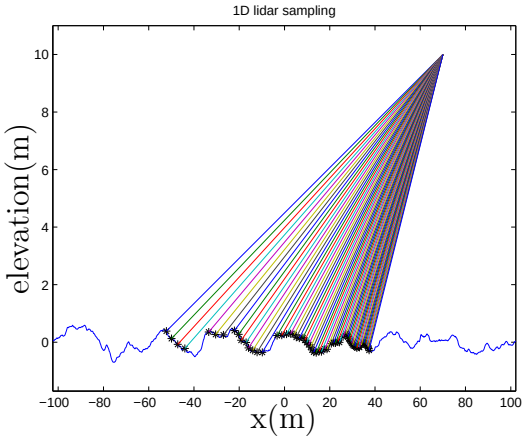

Figure 4 – Example of 1D LIDAR camera sampling of a nonlinear surface.

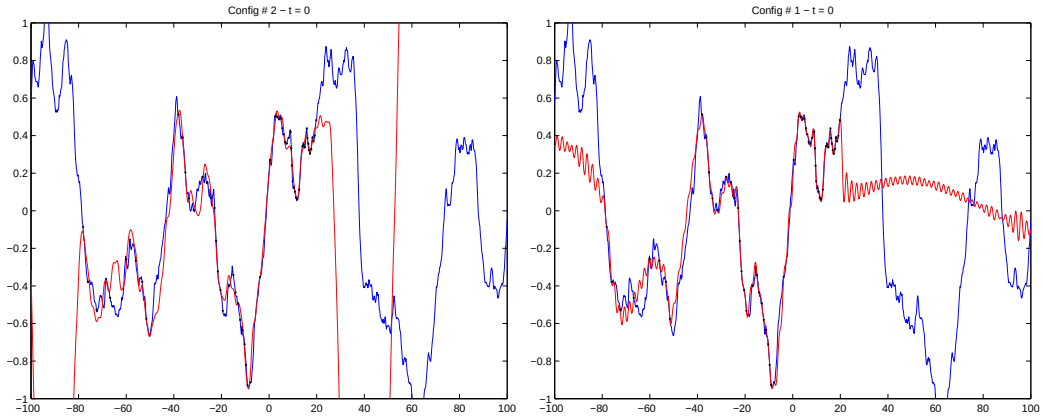

(a) (b)

Figure 5 – Linear reconstruction of a time evolving 1D CWM surface. Black dots a indicate observations on the simulated surface (blue lines). Red lines are reconstructed surfaces with $N_k = :$ (a) 40 ; (b) 400.

Additionally, we see that, despite the paucity of data for the more distant waves resulting from shadowing effects (which is an expected characteristics of LIDAR data), and particularly behind wave crests, the reconstructed surfaces capture well the salient features of the actual ocean surfaces, above the 2 m wavelength selected as the higher frequency cut-off in the algorithm However, as indicated before, the surface sampling process is strongly non-uniform and the density of sampled points on the sea surface is strongly decreasing with distance from the camera. Thus, the choice of the optimum number of reconstructed harmonics (N_k) is highly dependent on the Flash LIDAR illuminating configuration.

The relative error of the reconstruction is plotted as a function of N_k in Fig. 6 for the specific illuminating configuration used above, i.e.,

$$\epsilon = \sqrt{\sum_{l=1}^{N_v} (\eta_r - \eta_s)^2 \times \left[\sum_{l=1}^{N_v} (\eta_s - \overline{\eta}_s)^2 \right]^{-1}} \tag{18}$$

where η_s, η_r and $\overline{\eta}_s$ are respectively the simulated and reconstructed surfaces taken at each sampled point, and the mean elevation of the simulated surface. On Fig. 6, each marked data point was obtained by averaging the relative error over 10 test surfaces. We see that a good compromise between accuracy and computational time is obtained around $N_k = 400$ harmonics, which corresponds to about ten times the order of magnitude of observations points However, other simulations with higher wind speeds show that increasing N_k no longer improves reconstruction once the maximum wavelength becomes significantly larger than the camera's footprint size. This confirms that the camera configuration (e.g., aperture angle) must be adapted to wind conditions.

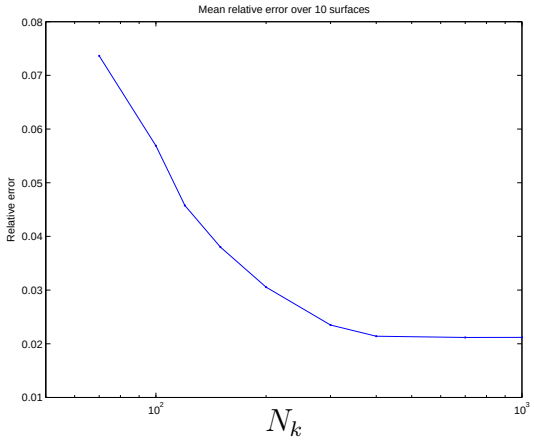

Figure 6 – Relative error of linear reconstruction versus number of harmonics

IV – 3 Reconstruction and prediction using time integration

At this point, our inversion scheme suffers from the fact that a data set obtained from a single snapshot of the surface at a given time does not provide enough information to discriminate between wave propagation directions (i.e., upwind or downwind in 1D). Doing so requires a time dependent data set, which has the additional advantage of making it possible to access some new points on the surface, which may have been hidden by a foreground wave crest at previous time steps.

As an example, we generated 1D LIDAR data sets, using the previous camera configuration, over a simulated nonlinear CWM surface with parameters : PM spectrum ;

$U_{19.5} = 7$ m.s^{-1} ; surface length of 200 m ; spatial step of 20 cm. We assumed that waves propagated in both positive and negative x directions in a dissymmetric manner with : 90% of the spectral energy associated with the wind direction (positive x) and 10% opposite to wind direction (negative x). Maximum and minimum wavelengths were respectively set to 45 m and 40 cm and the peak wave celerity to $c_p = 8$ m.s^{-1}. The LIDAR frequency of acquisition rate was set to 2 Hz, and thus a 64 point 1D data set would be obtained at each 0.5 second. The footprint of the LIDAR camera's aperture is about 100 m, as shown on Fig. 4. With 200 reconstructed harmonics spread over positive and negative wavenumbers, 5 to 7 iterations in CWM inversion algorithm are usually needed.

As remotely sensed waves are moving during time acquisition by the camera, it is no longer justified to define a relative error between simulated and reconstructed surfaces over the footprint area. As a practical objective of this project is to derive the best estimate of the sea state in front of a (moving) vessel, in order to derive the best way to steer through a given sea state, we define a new zone where the sea state estimate is useful for the vessel's path prediction. In the example below, we decided that this "prediction zone" was spanning about 20 m in front of the vessel (i.e., 20 m in front of the camera position) and the relative error of the reconstruction would thus be evaluated over this zone. Hence,

$$\epsilon = \frac{1}{\sigma_\eta}\sqrt{\frac{1}{N_z}\sum_{l=1}^{N_z}((\eta_r - \overline{\eta}_r^z) - (\eta_s - \overline{\eta}_s^z))^2}, \quad \text{with} \quad \sigma_\eta^2 = \frac{1}{N_v}\sum_{l=1}^{N_v}(\eta_s - \overline{\eta}_s)^2 \qquad (19)$$

where σ_η is the simulated surface variance, N_z is the number of simulated points in the "prediction zone" and N_v the total number of point of the simulated surface. $\overline{\eta}_r^z$ and $\overline{\eta}_s^z$ are respectively the mean surface elevation of the reconstructed and the simulated surfaces over the zone and prediction and $\overline{\eta}_s$ is the mean elevation of the whole simulated surface (usualy zero). Such a definition implies that the error is not sensitive to the wavelenghts greater than the zone of prediction size. We recall here that the free surface variance is related to the significant height as, $H_s = 4\sigma_\eta$. We tested 4 data sets, with different measuring times, from 0 to 12 seconds (i.e., 1 to 25 snapshots of the surface with a 2 Hz frequency data acquisition), and computed the relative errors, defined by Eq. (19), between the simulated and reconstructed surfaces.

In Fig. 7, the relative error over the "prediction zone" is plotted as a function of time. For instance, the red curve labelized $T_i = 8$ s means that data acquisition took place between $t = -8$ seconds and $t = 0$ seconds. At $t = 0$ s, remotely sensed waves have not yet reached the prediction zone and hence the simulated and reconstructed surfaces are still significantly different. Around $t = 15s$ most measured sensed waves have reached the "prediction zone" and the relative error reaches a minimum before increasing again once waves have passed by the vessel. Errors plotted in Fig. 7 are averaged over 40 nonlinear CWM surfaces, to obtain smoother curves.

Figure 7 shows that the prediction accuracy can not be as good as a mere inversion of a unique snapshot and is dependent on the acquisition time. First, the entire range of simulated wavelengths is not inverted and sensed wave are moving with different velocities which causes an unavoidable minimum error. An alternative error, defined for waves only belonging to the range of interest, could have been defined, but it could not be used in practical tests. However, Fig. 7 shows that a prediction is clearly possible and that time dependent data acquisition is a highly desirable for sea surface prediction. Error oscillations are related to a bad reconstruction of the low frequency part of the sea surface spectrum. Indeed, limited camera footprint size and limited time aquisition mainly

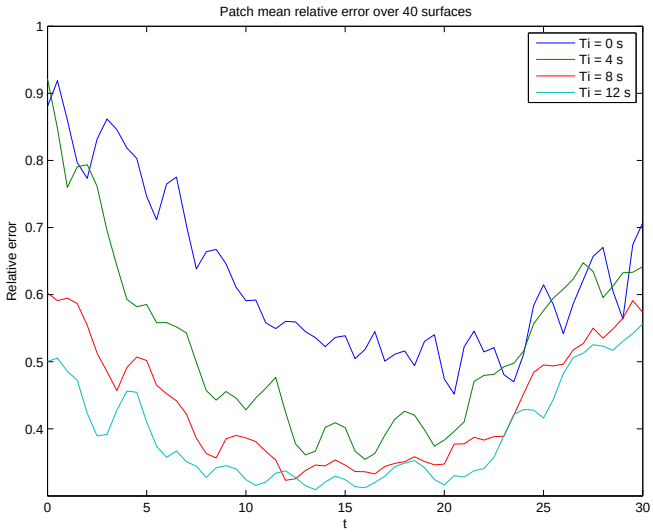

Figure 7 – Relative error versus forecasting time in the prediction zone. Aquisition frequency : 2 Hz

impact large scales reconstruction accuracy. In any case, higher the measurement time, the larger the prediction time window and the smaller the error. More precisely, if one wishes to predict the sea state "n" seconds in the future, one needs to observe waves in the wavelength range of interest, which will reach the"prediction zone" in "n" seconds. A continuous real time inversion will keep the relative error to the minimum level and is thus the best option. However, for vessel path prediction, sea state forecasting must be achieved for "prediction zones" near the camera footprint area, rather than close to the vessel's stern ; one would expect even smaller errors for these zones. Note, in practical applications, the useful forecasting zones will also be dependent upon vessel speed. a complete study of the inversion algorithm's performance as a function of all the parameters including vessel speed is left for future work.

Références

[1] C. Chae and J. Johnson. A study of interferometric phase statistics and accuracy for sea surface height retrievals from numerically simulated low-grazing-angle backscatter data. *Geoscience and Remote Sensing, IEEE Transactions on*, 49(99) :1–8, 2011.

[2] H. Dankert and W. Rosenthal. Ocean surface determination from x-band radar-image sequences. *Journal of geophysical research*, 109(C4) :C04016, 2004.

[3] R. Dean and R. Dalrymple. Water wave mechanics for engineers and scientists. *Prentice-Hall*, 1984.

[4] J. Johnson, R. Burkholder, J. Toporkov, D. Lyzenga, and W. Plant. A numerical study of the retrieval of sea surface height profiles from low grazing angle radar data. *Geoscience and Remote Sensing, IEEE Transactions on*, 47(6) :1641–1650, 2009.

[5] J. Nieto Borge, G. RodrÍguez, K. Hessner, and P. González. Inversion of marine radar images for surface wave analysis. *Journal of Atmospheric and Oceanic Technology*, 21(8) :1291–1300, 2004.

[6] F. Nouguier, C. Guérin, and B. Chapron. 'Choppy wave' model for nonlinear gravity waves. *Journal of Geophysical Research (Oceans)*, 114(C13) :09012, 2009.